

CMB Anisotropy Constraints on Open and Flat- Λ CDM Cosmogonies from UCSB South Pole, ARGO, MAX, White Dish, and SuZIE Data

Bharat Ratra¹, Radosław Stompor^{2,3}, Ken Ganga⁴, Graça Rocha³, Naoshi Sugiyama⁵, and Krzysztof M. Górski^{6,7}

ABSTRACT

We use combinations of ten small-scale cosmic microwave background anisotropy data sets from the UCSB South Pole 1994, ARGO, MAX 4 and 5, White Dish and SuZIE experiments to constrain cosmogonies. We consider open and spatially-flat- Λ cold dark matter cosmogonies, with nonrelativistic-mass density parameter Ω_0 in the range 0.1–1, baryonic-mass density parameter Ω_B in the range $(0.005\text{--}0.029)h^{-2}$, and age of the universe t_0 in the range (10–20) Gyr.

Marginalizing over all parameters but Ω_0 , the combined data favors an $\Omega_0 \simeq 1$ (1) open (flat- Λ) model. Excluding the smallest angular scale SuZIE data, an $\Omega_0 \simeq 0.3$ (1) open (flat- Λ) model is favored. Considering only multi-frequency data with error bars consistent with sample variance and noise considerations, i.e., the South Pole 1994 Ka band, the MAX 4 ι Draconis, and the MAX 5 HR5127 data, an $\Omega_0 \simeq 0.1$ (1) open (flat- Λ) model is favored. For both open and flat- Λ models and for all three combinations of data sets, after marginalizing over all the other parameters, a lower $\Omega_B h^2$ (~ 0.005) or younger ($t_0 \sim 10$ Gyr) universe is favored. However, the data do not rule out other values of Ω_0 in the flat- Λ model and other values of $\Omega_B h^2$ in both models. At 2σ confidence, model normalizations deduced from the small-scale data are consistent with those derived from the DMR data. We emphasize that since we consider only a small number of data sets, these results are tentative.

Subject headings: cosmic microwave background—cosmology: observations—large-scale structure of the universe

¹Department of Physics, Kansas State University, Manhattan, KS 66506.

²Institute of Astronomy, University of Cambridge, Madingley Road, Cambridge, CB3 0HA, UK.

³Copernicus Astronomical Center, Bartycka 18, 00-716 Warszawa, Poland.

⁴IPAC, MS 100–22, California Institute of Technology, Pasadena, CA 91125.

⁵Department of Physics, Kyoto University, Kitashirakawa-Oiwakecho, Sakyo-ku, Kyoto 606-8502, Japan.

⁶Theoretical Astrophysics Center, Juliane Maries Vej 30, 2100 Copenhagen Ø, Denmark.

⁷Warsaw University Observatory, Aleje Ujazdowskie 4, 00-478 Warszawa, Poland.

1. Introduction

Six years ago the *COBE*-DMR experiment detected anisotropy in the cosmic microwave background (CMB) on angular scales $\sim 10^\circ$ (Smoot et al. 1992; Wright et al. 1992; Bennett et al. 1996; Górski et al. 1996). Since then a number of experiments have measured the anisotropy on smaller angular scales, down to arcminutes (Ganga et al. 1994; Gutiérrez et al. 1997; Femenía et al. 1998; Netterfield et al. 1997; Gundersen et al. 1995; Tucker et al. 1997; de Oliveira-Costa et al. 1998; Platt et al. 1997; Masi et al. 1996; Lim et al. 1996; Cheng et al. 1997; Griffin et al. 1999; Baker et al. 1998; Leitch et al. 1998; Church et al. 1997; Subrahmanyam et al. 1998).

These observations are becoming an increasingly powerful tool for testing cosmogonies and constraining cosmological parameters such as Ω_0 , h , and Ω_B in these models⁸. While definitive results will probably have to await new data acquired at a variety of frequencies to constrain or estimate possible non-CMB anisotropy foreground emission, it is of interest to explore what constraints current data place on cosmological model parameters. Given the error bars associated with current measurements, interesting constraints on cosmological model parameters require simultaneous use of many data sets in this exploration.⁹ Two distinct techniques have been used to combine results from different data sets.

In the first approach, a goodness-of-fit (“ χ^2 ”) comparison of CMB anisotropy predictions, which depend on model parameters, and observational results is used to constrain cosmological model parameters (e.g., Ganga, Ratra, & Sugiyama 1996; Hancock et al. 1998; Lineweaver et al. 1997; Lineweaver & Barbosa 1998; Baker et al. 1998). This comparison does not make use of the complete data from each experiment. Rather, it typically uses a single number (amplitude of a predefined CMB spectrum) with error bars, derived from the rms anisotropy measured by the experiment. As a consequence it is an easily used technique that allows for a rapid exploration of cosmological parameter space. On the other hand it does have a number of significant drawbacks, some of which are discussed, most recently, by Bond, Jaffe, & Knox (1998) and by Tegmark (1998). In particular, the amplitude (and error bars) used to represent the data is model dependent — this is typically a $\sim 10\%$ effect for current data sets with good detections (Ganga et al. 1997a, hereafter GRGS; Ganga et al. 1998; Ratra et al. 1999, hereafter R99). This is not accounted for in the χ^2 analyses, since they use an amplitude (and error bars) extracted from the data on the basis of an assumed flat bandpower spectrum or gaussian autocorrelation function. More importantly, these amplitudes and error bars are derived from quite nongaussian posterior probability density distribution functions. As a result the observational error bars are quite asymmetric and symmetrizing (“gaussianizing”) them in different ways results in different χ^2 values (Ganga et al. 1996). Note that gaussianization is mandatory, not optional, for the χ^2 technique. Furthermore,

⁸ Here Ω_0 is the nonrelativistic-mass density parameter, h is the Hubble parameter in units of $100 \text{ km s}^{-1} \text{ Mpc}^{-1}$, and Ω_B is the baryonic-mass density parameter.

⁹ It is important to use as many data sets as possible, and to not rely on just a few, since any data set could be biased by an as-yet undiscovered systematic effect.

the χ^2 technique, as currently applied, can not account for observational upper limits. As discussed below, at least one upper limit (SuZIE) significantly constrains cosmological parameter space. In addition, when assigning confidence limits on cosmological parameters to the constant χ^2 bounds, proponents of the χ^2 technique assume that the resulting probability distribution is a gaussian function of the cosmological parameters, which is not true. Given these drawbacks it is clear that one should not rely solely on the χ^2 technique for quantitative constraints on cosmological parameters. We note, however, that the technique does qualitatively establish that the CMB anisotropy spectrum has more power on smaller angular scales (Ganga et al. 1996), consistent with recent Saskatoon observations (Netterfield et al. 1997).

The second and more correct approach, a joint maximum likelihood analysis of all the data sets using realistic model anisotropy spectra, is very time consuming. This approach has been used to constrain cosmological parameters on the basis of a single data set (Bunn & Sugiyama 1995; Górski et al. 1995, 1998; Stompor, Górski, & Banday 1995; Yamamoto & Bunn 1996; GRGS; Ganga et al. 1997b, 1998; Bond & Jaffe 1997; Stompor 1997; Ratra et al. 1998; R99), and a combination of three data sets (Bond & Jaffe 1997). Such analyses use the full information in each data set, rather than the single amplitude with error bars used in the χ^2 analyses.

In this paper we combine results from earlier analyses of the Gundersen et al. (1995) UCSB South Pole 1994 data, the Church et al. (1997) SuZIE data, the MAX 4 and 5 data (Tanaka et al. 1996; Lim et al. 1996), the Tucker et al. (1993) White Dish data, and the de Bernardis et al. (1994) ARGO Hercules data.¹⁰ These analyses made use of theoretically-predicted CMB anisotropy spectra in open and flat- Λ cold dark matter (CDM) models (GRGS; Ganga et al. 1997b, 1998; Ratra et al. 1998; R99). Since these data sets were acquired from regions that are well separated in space, the likelihoods of the individual data sets are independent and can thus be multiplied together to construct the likelihood of the combined data set. This combined likelihood is then used to derive constraints on cosmological model parameters.

Our analysis here is complementary to that of Bond & Jaffe (1997). They consider the DMR, UCSB South Pole 1994, and Saskatoon data sets and develop a method to constrain cosmological parameters, while we focus here on a larger number of smaller angular scale data sets. To cut down on complexity, we do not consider the DMR data in this paper. Different ways of dealing with the quadrupole moment in the DMR analysis lead to significantly different constraints on cosmological parameters (Górski et al. 1998), so a proper treatment would require consideration of at least two different sets of DMR results, leading to a significant increase in the number of data set combinations (since we consider various combinations of the small-scale data sets) and a proliferation of figures. We also want to first focus on the constraints from smaller angular scale data, and, in particular, compare results from different combinations of the small-scale data sets. While we consider fewer model parameters than did Bond & Jaffe — for instance, we do not allow

¹⁰ We use this set of data as a test case to develop the method, since these are the results we currently have access to.

for tilt, gravity waves, or hot dark matter — we explore, in a systematic way, a much broader range for the model parameters considered. Also, unlike Bond & Jaffe, we perform a likelihood analysis of the complete data, i.e., we do not use data compression to speed up the computation and minimize memory requirements.

In §2 we describe the models and cosmological parameter space we consider. See R99 for further details. In §3 we discuss the various combinations of data sets we consider. In §4 we summarize the computational techniques we use. See GRGS for a more detailed description. Results are presented and discussed in §5 and we conclude in §6.

2. Cosmogonical Models

Current data are most easily accommodated in a low-density cosmogony. These data include:

- Dynamical estimates of the mass clustered on scales $\lesssim 10 h^{-1}$ Mpc, which suggest a low Ω_0 . For example, virial analysis of X-ray cluster data indicates $0.07 \leq \Omega_0 \leq 0.31$ at 2σ (Carlberg et al. 1997a). Some of the mass might not cluster on these small scales, so these estimates might be biased low. However, recent dynamical estimates of the mass clustered on large scales $\gtrsim 10 h^{-1}$ Mpc indicate $0.1 \lesssim \Omega_0 \lesssim 0.6$ at $\sim 2 \sigma$ (e.g., Willick et al. 1997; Borgani et al. 1997, also see Small et al. 1998).
- Low estimates of Ω_0 from measurements of the baryonic-mass fraction of the rich clusters, standard nucleosynthesis, and the observed light-element abundances (e.g., Evrard 1997; Ettori, Fabian, & White 1997).
- The redshift $z \sim 0$ masses and abundances of galaxy clusters, which indicate $0.25 \lesssim \Omega_0 \lesssim 0.5$ in DMR-normalized CDM cosmogonies (e.g., Cole et al. 1997).
- The shape of the observed galaxy fluctuation power spectrum (e.g., Maddox, Efstathiou, & Sutherland 1996).
- The lack of large evolution in the galaxy cluster luminosity function, to $z \sim 0.5$, which indicates $0.2 \lesssim \Omega_0 \lesssim 0.6$ at 1.6σ in CDM models (e.g., Carlberg et al. 1997b; Ebeling et al. 1997; Mushotzky & Scharf 1997; Bahcall, Fan, & Cen 1997; Eke et al. 1998, also see Voit & Donahue 1998).
- Indications of high- z structure formation, e.g., massive clusters at $z \sim 0.5 - 1$ (e.g., Deltorn et al. 1997; Donahue et al. 1998), similarity between the giant elliptical luminosity function at $z \sim 1$ and the present (e.g., Gardner et al. 1997; Small, Sargent, & Hamilton 1997, also see van Dokkum et al. 1998), massive galactic disks at $z \sim 1$ (Vogt et al. 1996), and galaxy groups at $z > 2$ (e.g., Francis, Woodgate, & Danks 1997).

The simplest low-density CDM cosmogonies have either flat spatial hypersurfaces and a cosmological constant Λ , or open spatial hypersurfaces and no Λ . Both these low density models are consistent with the data mentioned above. For recent discussions see Park et al. (1998), Peebles (1998), Retzlaff et al. (1998), Colín et al. (1998), Croft et al. (1998), and Governato et al. (1998). There is additional data which favors either the flat- Λ or the open model.

The data which favors the open model include:

- Measurements of the Hubble parameter which suggest $h = 0.65 \pm 0.1$ at 2σ (e.g., Giovanelli et al. 1997; Hjorth & Tanvir 1997; Falco et al. 1997; Della Valle et al. 1998), and measurements of age of the universe which indicate $t_0 = 12 \pm 2.5$ Gyr at 2σ (e.g., Feast & Catchpole 1997; Reid 1997; Gratton et al. 1997; Chaboyer et al. 1998). The resulting central $H_0 t_0$ value is consistent with an open model with $\Omega_0 \approx 0.35$ and a flat- Λ model with $\Omega_0 \approx 0.6$, somewhat larger than what is favored by the data above. At 2σ there is no significant constraint on Ω_0 in the open model, but $\Omega_0 \gtrsim 0.25$ is required in the flat- Λ model.
- Analyses of the rate of gravitational lensing of quasars and radio sources by foreground galaxies requires $\Omega_0 \geq 0.38$ at 2σ in the flat- Λ model but only weakly constrains the open case (e.g., Bloomfield Torres & Waga 1996; Kochanek 1996; Falco, Kochanek, & Muñoz 1998; Jain et al. 1998).¹¹
- The predicted number of large arcs formed by strong gravitational lensing by clusters in the open model is more consistent with what is observed (Bartelmann et al. 1998).
- When normalized to the DMR observations, the flat- Λ CDM model with a scale-invariant spectrum has excessive intermediate- and small-scale power and hence requires mild antibiasing, which is not easily reconciled with the observations (e.g., Stompor et al. 1995; Liddle et al. 1996; Cole et al. 1997).

In passing, we note that most of these observations can probably be reconciled with a time-variable cosmological “constant” dominated spatially-flat model (e.g., Peebles & Ratra 1988; Sugiyama & Sato 1992; Ratra & Quillen 1992; Coble, Dodelson, & Frieman 1997; Ferreira & Joyce 1997; Caldwell, Dave, & Steinhardt 1998; Viana & Liddle 1998; Frieman & Waga 1998; Anderson & Carroll 1998; Özer & Taha 1998; Huterer & Turner 1998; Starobinsky 1998).

On the other hand, recent applications of the apparent magnitude versus redshift test using Type Ia supernovae favor the flat- Λ model (e.g., Riess et al. 1998; Perlmutter et al. 1999).

We emphasize that some, if not most, of the above constraints are very tentative. They should be viewed as indicative as what may soon be possible, and are certainly not definitive.

¹¹ It has recently been suggested that systematic uncertainties currently preclude a strong constraint on Λ from the gravitational lensing of quasars (Cheng & Krauss 1998). The constraint using only radio data is still quite restrictive, $\Omega_0 \geq 0.27$ at 2σ (Falco et al. 1998).

In the analyses in this paper we focus on a spatially open CDM model and a spatially flat CDM model with a Λ . These models have gaussian, adiabatic primordial energy-density power spectra. The flat- Λ model CMB anisotropy computations use a scale-invariant energy-density perturbation power spectrum (Harrison 1970; Peebles & Yu 1970; Zel’dovich 1972), as predicted in the simplest spatially-flat inflation models (Guth 1981; Kazanas 1980; Sato 1981a, 1981b). The open model computations use the energy-density power spectrum (Ratra & Peebles 1994, 1995; Bucher, Goldhaber, & Turok 1995; Yamamoto, Sasaki, & Tanaka 1995) predicted in the simplest open-bubble inflation models (Gott 1982; Guth & Weinberg 1983).

To make the problem tractable, in each model (open and flat- Λ) we consider anisotropy spectra parameterized by (i) the quadrupole-moment amplitude $Q_{\text{rms-PS}}$, (ii) Ω_0 , (iii) $\Omega_B h^2$, and (iv) t_0 . While it is of interest to also consider other cosmological parameters, current data does not justify the effort needed to explore a larger dimensional parameter space. In particular, in our analyses here we ignore the effects of tilt, primordial gravity waves, and reionization. These effects are unlikely to be very significant in viable open models although they could help reconcile some flat- Λ model predictions with the observations. More specifically, while we do not use goodness-of-fit statistics in this paper to check whether the favored cosmological parameter values derived here are a good fit to the data, χ^2 analyses have qualitatively shown that some of the models in the four-dimensional parameter space we study in this paper are indeed a good fit to the data, possibly better than should be expected (Ganga et al. 1996; Lineweaver & Barbosa 1998; Tegmark 1998). That is, current data does not require consideration of a larger dimensional parameter space. In addition, we note that constraints on model parameters from each of the individual data sets used in this paper are largely mutually consistent.

The computation of the anisotropy spectra is described in Stompor (1994) and Sugiyama (1995). We have evaluated the spectra for a range of Ω_0 spanning the interval 0.1 to 1 in steps of 0.1, for a range of $\Omega_B h^2$ spanning the interval 0.005 to 0.029 in steps of 0.004, and for a range of t_0 spanning the interval 10 to 20 Gyr in steps of 2 Gyr. See R99 for further details. Figure 1 shows examples of the model CMB anisotropy spectra used in our analyses. Other examples are shown in Figure 2 of R99.

3. CMB Anisotropy Data Sets

We consider various combinations of ten different data sets. The data sets we use are the UCSB South Pole 1994 Ka and Q band observations, hereafter SP94Ka and SP94Q (Gundersen et al. 1995; GRGS)¹², the ARGO Hercules observations (de Bernardis et al. 1994; R99), the MAX 4 ι Draconis (ID) and σ Herculis (SH) and MAX 5 HR5127 (HR), μ Pegasi (MP), and ϕ Herculis (PH) observations (Tanaka et al. 1996; Lim et al. 1996; Ganga et al. 1998), the White Dish

¹² Note that our analysis of the full SP94 data set accounts for all the correlations.

observations (Tucker et al. 1993; Ratra et al. 1998), and the SuZIE observations (Church et al. 1997; Ganga et al. 1997b). Detailed information about these data sets may be found in the papers cited above; in what follows we discuss only directly relevant issues.

Amongst the experiments we consider, the SuZIE observations probe the smallest angular scales. In some models SuZIE is still quite sensitive to multipoles $l \sim 2000$ (Ganga et al. 1997b). On these angular scales a number of effects not accounted for in our CMB anisotropy power spectra computations can modify the primordial CMB anisotropy power spectra. We therefore consider combined data sets both including and excluding the SuZIE observations, so as to bias our conclusions as little as possible.

Multifrequency data sets, such as SP94 and MAX 4 and 5, allow for an “internal” estimate of the amount of non-CMB anisotropy foreground contamination. In this sense they are “better” than single frequency data sets.

Besides the well-known spectral analysis method for checking for foreground contamination, some multifrequency data sets allow one to use sample variance and noise considerations to check for consistency of the data with CMB anisotropy (GRGS, pp. 19–21). The method is as follows; see GRGS for a detailed discussion and GRGS and Ganga et al. (1998) for applications of the method. If systematic uncertainties (such as those in the beamwidth, calibration, or pointing) are small, the deduced $Q_{\text{rms-PS}}$ error bars only account for noise and sample variance. Assuming that the data is pure CMB anisotropy, when individual channel observations are combined, the noise contribution to the error bars will integrate down in known fashion while the sample variance contribution will not (since the sky coverage does not change). Since the behavior of the noise part of the error bars is known, comparing the error bars derived from each of the individual channel observations to those derived from the combined data allows for an estimate of the sample variance directly from the data. If this estimate of the sample variance is consistent with that estimated independently from the observing strategy and parameters of the instrument, it is reasonable to conclude that the data is not inconsistent with CMB anisotropy.

Spectral analyses and simple analytic sample variance estimates indicate that the SP94Ka and MAX 5 HR data are more consistent with what is expected for CMB anisotropy than are the SP94Q and MAX 5 PH data (GRGS; Ganga et al. 1998, also see Tanaka et al. 1996)¹³. While the MAX 5 PH observations were done at lower balloon altitude and so through more of the atmosphere (Tanaka et al. 1996), and while there is indication of a possible non-CMB foreground in other Q band observations made at Saskatoon (de Oliveira-Costa et al. 1997), it is useful to improve on the simple analytic sample variance estimates of GRGS and Ganga et al. (1998) to see if their conclusions are justified.

To improve upon these estimates we have generated 1000 Monte Carlo maps of the flat

¹³ Given the error bars, the spectral analysis can not be used to argue that the SP94Q data is not purely CMB anisotropy (GRGS).

bandpower CMB anisotropy in a flat two-dimensional space¹⁴. We then mimic the SP94 and MAX 4 and 5 observational techniques and “observe” these noise-less simulations.

For the SP94 Ka and Q observations we find sample variances of 23% and 22% of the bandtemperature, estimated at the central beamwidths, as in the GRGS sample variance estimate. These are larger than the 21% and 18% estimated by GRGS on the basis of the simple analytic formula. However, the conclusions of GRGS are unaffected. That is, given these new numerical estimates of sample variance, the SP94Ka data is still more consistent with what is expected for CMB anisotropy than is the SP94Q data.

For MAX 5 we find a sample variance of 23%, estimated at beamwidth $\sigma_{\text{fwhm}} = 0.5^\circ$, as in the Ganga et al. (1998) sample variance estimate. This is larger than the Ganga et al. (1998) analytic estimate of 19%. However, this is not large enough to affect the Ganga et al. (1998) conclusion that the MAX 5 HR error bars are more consistent with what is expected for CMB anisotropy than are the MAX 5 PH ones. We also note that MAX 5 MP data has structure that correlates with *IRAS* 100 μm dust emission (Lim et al. 1996). Since the MAX 4 SH error bars do not significantly shrink when the individual channel observations are combined, while the MAX 4 ID error bars do, Ganga et al. (1998) concluded that the MAX 4 SH data was not that consistent with what is expected for CMB anisotropy, while MAX 4 ID could be.

On the basis of these, admittedly weak, arguments, we therefore also analyze the combination of SP94Ka, MAX 4 ID, and MAX 5 HR data. These are multifrequency observations with error bars consistent with what is expected for CMB anisotropy on the basis of sample variance and noise considerations. More precisely, these three data sets are the only ones (amongst those considered in this paper) for which we have no basis to suspect foreground contamination.¹⁵ In this sense this is a conservative combination of data. We emphasize, however, that some or all of the other data sets could also be purely CMB anisotropy, since our arguments do not establish the contrary at a convincing statistical level.

We emphasize that a proper treatment would require a complete analysis of each individual data set, accounting for a CMB anisotropy signal as well as various non-CMB foreground signals. Since there almost certainly are uncharacterized non-CMB foregrounds, this is likely to be a difficult undertaking.

In summary, then, we consider three different combinations of data sets: i) all data (SP94, ARGO, MAX 4 and 5, White Dish, and SuZIE); ii) all data excluding SuZIE; and iii) SP94Ka, MAX 4 ID, and MAX 5 HR data.

¹⁴ The SP94 and MAX 4 and 5 experiments probe a small enough region of the sky for the flat space approximation to hold.

¹⁵ While there are notable exceptions, we emphasize that other data at similar angular scales tend to have a larger amplitude.

4. Summary of Computation

GRGS describe the computation of the likelihood function for a given CMB anisotropy data set. Offsets and gradients removed from the data are accounted for in the analysis. Beamwidth and calibration uncertainties are also accounted for as described in GRGS.

The likelihood functions for the individual data sets considered in this paper were recomputed in R99, for the much larger set of cosmogonical model spectra considered here. The initial models-based analyses, except for ARGO, used only 25 model spectra (Ratra et al. 1997), in contrast to the 798 considered here. Since the data sets considered are well separated in space, and in some cases also in angular resolution, the likelihood functions of the individual data sets are simply multiplied together to construct the likelihood function of the combined data. These open and flat- Λ model likelihoods are a function of four parameters: $Q_{\text{rms-PS}}$, Ω_0 , $\Omega_B h^2$, and t_0 . Marginalized likelihood functions are derived by integrating over one or more of these parameters. We assume a uniform prior in the parameters integrated over, set to zero outside the parameter range considered.

To determine central values and limits from the likelihood functions we assume a uniform prior in the relevant parameter. Then the corresponding posterior probability density distribution function vanishes outside the chosen parameter range and is equal to the likelihood function inside this range. The deduced central value of the parameter is taken to be the value at which the posterior probability density peaks, and we quote highest posterior density (HPD) limits. See GRGS and R99 for details. The quoted limits depend on the prior range considered for the parameter. This is a significant effect if the likelihood function is not sharply peaked within the parameter range considered, as is the case for a number of the likelihood functions derived in this paper. See R99 for a more detailed discussion of this issue.

5. Results and Discussion

For the flat bandpower spectrum, the posterior distribution for the combined data peaks at $Q_{\text{rms-PS}} = 25 \mu\text{K}$, with a 1σ range of $23 \mu\text{K} < Q_{\text{rms-PS}} < 27 \mu\text{K}$, resulting in an averaged fractional 1σ uncertainty of 8.9%, and with likelihood ratio¹⁶ = 4×10^{99} . For this spectrum, the posterior distribution for the combined data excluding SuZIE peaks at $Q_{\text{rms-PS}} = 26 \mu\text{K}$, with 1σ range of $24 \mu\text{K} < Q_{\text{rms-PS}} < 29 \mu\text{K}$, resulting in an averaged fractional uncertainty of 9.5%, and with likelihood ratio = 7×10^{99} . For the SP94Ka, MAX 4 ID, and MAX 5 HR data combination, the posterior distribution peaks at $Q_{\text{rms-PS}} = 22 \mu\text{K}$, with 1σ range of $18 \mu\text{K} < Q_{\text{rms-PS}} < 26 \mu\text{K}$, resulting in an averaged fractional uncertainty of 19%, and with likelihood ratio = 1×10^{31} . These numerical values account for beamwidth and calibration uncertainties, and the removal of

¹⁶ This is the ratio of the value of the posterior distribution at the peak to that at $Q_{\text{rms-PS}} = 0 \mu\text{K}$.

offsets and gradients when appropriate. Clearly, these combined data sets result in very significant detections of CMB anisotropy, even after known systematic uncertainties are accounted for. We emphasize that the most conservative combination (SP94Ka, MAX 4 ID, and MAX 5 HR) has a lower amplitude than the other two data combinations, but it is not significantly lower. Also, while this most conservative combination of data has a larger error bar, 19%, qualitatively consistent with a smaller amount of data, adding additional data to that considered here should result in a considerably smaller error bar. For comparison, the corresponding DMR error bar is $\sim 10 - 12\%$ (depending on model, Górski et al. 1998).

As for ARGO (R99), for both the open and flat- Λ models, the four-dimensional posterior probability density distribution function $L(Q_{\text{rms-PS}}, \Omega_0, \Omega_B h^2, t_0)$ is nicely peaked in the $Q_{\text{rms-PS}}$ direction but fairly flat in the other three directions (especially in the $\Omega_B h^2$ and t_0 directions). Again as for ARGO (R99), marginalizing over $Q_{\text{rms-PS}}$ results in a three-dimensional posterior distribution $L(\Omega_0, \Omega_B h^2, t_0)$ which is steeper. Since the limits determined from the four- and three-dimensional posterior distributions are not highly statistically significant, we do not show detailed contour plots of these functions here. However, the vertical heavy solid lines in Figure 8 show the formal 1σ and 2σ confidence limits derived by projecting the appropriate four-dimensional posterior distribution on to the $Q_{\text{rms-PS}}$ axis. These limits are reasonably close together in the $Q_{\text{rms-PS}}$ direction, illustrating the steepness of the four-dimensional posterior distribution in this direction.

Marginalizing over $Q_{\text{rms-PS}}$ and one other parameter results in two-dimensional posterior probability functions which are more peaked. Some examples are shown in Figures 2–4. Again as for ARGO (R99), in some cases these peaks are at an edge of the parameter range considered. Figures 2–4 illustrate a number of interesting points, some of which we return to below when we discuss the posterior distribution obtained by marginalizing over one more parameter, i.e., the posterior distributions for each of the four parameters.

Figure 4 shows results in the $(Q_{\text{rms-PS}}, \Omega_0)$ plane for the open model and the individual MAX 4 ID, MAX 5 HR, and SP94Ka data sets, as well as the combined SP94Ka, MAX 4 ID, and MAX 5 HR data set. Panels *a) – c)* show that the contours of the posterior distribution in the Ω_0 direction for these three individual data sets look like rescaled (in $Q_{\text{rms-PS}}$) versions of each other. This is partly because the three experiments probe similar angular scale parts of the model CMB power spectra, the multipole $l \sim 50 - 100$ rise towards the first peak, which are only weakly dependent on Ω_0 (see Figure 1), and partly because the data error bars are large. As a result, when one does a joint analysis of the three data sets the contours in the $Q_{\text{rms-PS}}$ direction are closer together while those in the Ω_0 direction do not shift as significantly. Thus a combined analysis of the data sets results in tighter limits on $Q_{\text{rms-PS}}$ but not significantly stronger constraints on Ω_0 .

This effect has previously been noticed by GRGS, Bond & Jaffe (1997), Ganga et al. (1998), and R99. GRGS found that when the SP94 Ka and Q data were jointly analyzed the limits on $Q_{\text{rms-PS}}$ were somewhat tighter than those derived from the Ka or Q data alone while the

combined data did not better differentiate between different Ω_0 values than did the individual data sets. Ganga et al. (1998) also drew attention to this effect in their joint analysis of the MAX 4 and 5 data. Figure 5 of R99 shows posterior density distribution contours in the $(Q_{\text{rms-PS}}, \Omega_0)$ plane for the DMR, SP94, ARGO, MAX 4 and 5, White Dish, and SuZIE data.

Bond & Jaffe (1997) use the amplitude of mass fluctuations at $8h^{-1}$ Mpc, $\delta M/M(8h^{-1} \text{ Mpc})$, instead of $Q_{\text{rms-PS}}$, and show posterior density distribution contours in the $(\delta M/M(8h^{-1} \text{ Mpc}), n)$ and $(\delta M/M(8h^{-1} \text{ Mpc}), h)$ planes instead of the plots we show. (Here n is the primordial energy-density perturbation power spectral index.) They consider the combination of the DMR, SP94, and Saskatoon data, and point out that since the DMR data does constrain n fairly well (Górski et al. 1996) but not h (e.g., Górski et al. 1998), the combination of DMR, SP94, and Saskatoon data does constrain n fairly well, but not h . A similar constraint on Ω_0 in the open models at low Ω_0 (as that on n) would be expected from the SuZIE data (and to a lesser extent from the DMR data) — see Figure 5 panels *h*) and *b*) of R99, and Figure 3 panels *b*) and *d*) of this paper.

Figure 2 shows that the two-dimensional posterior distributions allow one to distinguish between different regions of parameter space at a fairly high formal level of confidence. For instance, for the SP94Ka, MAX 4 ID, and MAX 5 HR data combination (panels *c*) and *f*) in the bottom row), the open model near $\Omega_0 \sim 0.7$, $\Omega_B h^2 \sim 0.03$, and $t_0 \sim 20$ Gyr, and the flat- Λ model near $\Omega_0 \sim 0.45$, $\Omega_B h^2 \sim 0.03$, and $t_0 \sim 20$ Gyr, are both formally ruled out at $\sim 3 \sigma$ confidence. However, we emphasize, as discussed below, care must be exercised when interpreting the discriminative power of these formal limits, since they depend sensitively on the fact that the uniform prior has been set to zero outside the range of the parameter space we have considered.

Figure 3 shows the contours of the two-dimensional posterior distribution for $Q_{\text{rms-PS}}$ and Ω_0 , derived by marginalizing the four-dimensional distribution over $\Omega_B h^2$ and t_0 . These are shown for the three combined small-scale data sets and the DMR data, for both the open and flat- Λ models. At 2σ confidence, constraints on these parameters derived from the three combined small-scale data sets are mostly consistent with those derived from the DMR data. However, at a lower level of significance, the DMR data favor a higher normalization for the flat- Λ model than do the combined small-scale data sets, see panels *a*), *c*), and *e*) of Figure 3. It is interesting that the constraints on $Q_{\text{rms-PS}}$ derived from the DMR data are not much tighter than those derived from the combined small-scale data sets. A similar conclusion has previously been drawn from the MAX 4 and 5 data alone (Ganga et al. 1998) and the ARGO data alone (R99). As mentioned above, excluding SuZIE from the combined small-scale data set results in an increase of the allowed low- Ω_0 region for the open model, see panels *b*) and *d*) of Figure 3.

Figure 5 shows the one-dimensional posterior distribution functions for Ω_0 , derived by marginalizing the four-dimensional ones over the other three parameters. For the flat- Λ model (left hand column of Figure 5), all three combinations of data sets favor $\Omega_0 = 1$, although no value of Ω_0 is ruled out since the distributions are quite flat. Including or excluding the SuZIE data,

panels *a*) and *c*), hardly changes the posterior distribution for the flat- Λ model. This is mostly a consequence of the fact that the flat- Λ models do not predict much CMB anisotropy power on the angular scales probed by SuZIE (see Figure 1). The results for the open model (right hand column of Figure 5) are dramatically different. Using all the data, panel *b*), $\Omega_0 = 1$ is favored, with, formally, $\Omega_0 > 0.55$, > 0.28 , and > 0.1 at 1σ , 2σ , and 3σ confidence, respectively. Excluding SuZIE, panel *d*), significantly shifts the most likely value to $\Omega_0 = 0.28$. Considering only the SP94Ka, MAX 4 ID, and MAX 5 HR combination, panel *f*), the most favored open model is at $\Omega_0 = 0.1$ with $0.47 < \Omega_0 < 0.87$ formally excluded at 1σ and $0.63 < \Omega_0 < 0.71$ formally excluded at 2σ .

As mentioned above, and discussed in the analysis of the ARGO data (R99), care is needed when interpreting the discriminative power of these formal limits. If the posterior density function was a gaussian which peaked well inside the parameter range considered, the 1 , 2 , and 3σ HPD limits would correspond to a value of the posterior distribution relative to that at the peak of 0.61 , 0.14 , and 0.011 respectively. Using this criterion, the posterior distribution of Figure 5*b*), for the open model and all the small-scale data, sets a 2σ confidence limit of $\Omega_0 \gtrsim 0.2$ and a 3σ confidence limit of $\Omega_0 \gtrsim 0.1$. This gaussian posterior ratio criterion also results in a 1σ confidence limit of $\Omega_0 \lesssim 0.3$ for the open model and the SP94Ka, MAX 4 ID, and MAX 5 HR combination, panel *f*). This criterion does not result in 1σ limits for any of the other panels.

To summarize, the most conservative constraints follow from the SP94Ka, MAX 4 ID, and MAX 5 HR data combination, Figure 5 panels *e*) and *f*) — the most favored value is $\Omega_0 = 0.1$ (1) for the open (flat- Λ) model, with $\Omega_0 \gtrsim 0.3$ excluded at 1σ for the open model and no constraint on the flat- Λ model if the gaussian posterior distribution ratio criterion is used. That is, even using this most conservative prescription a 1σ limit can be set on Ω_0 in the open model, and the most favored open model is somewhat more favored than the most favored flat- Λ one.

While the inclusion or exclusion of the SuZIE data do not significantly affect the flat- Λ models constraints, panels *a*) and *c*) of Figure 5 or panels *a*) and *c*) of Figure 3, it does significantly affect the open model constraints, panels *b*) and *d*) of Figure 5 or panels *b*) and *d*) of Figure 3, shifting the most likely value of Ω_0 from 1 to 0.3. Since the SuZIE data only results in an upper limit (Church et al. 1997; Ganga et al. 1997b), it is not straightforward to include it in a conventional goodness-of-fit (χ^2) analysis. This is a drawback of the conventional χ^2 technique.

It is of interest to compare the constraints on Ω_0 in the open model from the combined SP94Ka, MAX 4 ID, and MAX 5 HR analysis¹⁷ with what has been derived from χ^2 analyses which include much more data. As mentioned above, we find, from Figure 5*f*), that $\Omega_0 = 0.1$ is the most favored value, with the conservative gaussian posterior distribution ratio upper limit of $\Omega_0 \lesssim 0.3$ at 1σ and no constraint at 2σ . This is not inconsistent with the Ganga et al.

¹⁷ We again emphasize that these results are tentative since we consider only three data sets. Also, as noted above, other data at similar angular scales tend to have a larger amplitude.

(1996) χ^2 analysis conclusion that $\Omega_0 \sim 0.4 - 0.5$ is favored. It is also not inconsistent with the Baker et al. (1998) values $\Omega_0 = 0.7^{+0.6}_{-0.4}$ at 2σ , where we have simply doubled their 1σ error bars. However, it seems to be difficult to reconcile this with the Lineweaver & Barbosa (1998) conclusion that $\Omega_0 > 0.3$ at more than $\sim 4\sigma$ confidence (if $h = 0.7$). This difference could be due to a number of effects. It could be due to the fact that we have considered only a small number of data sets. Another possibility is the different numerical values ascribed to some of the data sets in the two analyses. For instance, recent reanalyses (GRGS; Ganga et al. 1997b, 1998; Ratra et al. 1998; R99) of some of the data, which more carefully accounts for systematic effects, has altered a number of data points, some quite significantly. Yet another possibility is that some of the data sets considered in the χ^2 analysis but not in this paper are inconsistent with the data sets considered here, for the restricted four-dimensional parameter space we have studied. This, however, does not seem very likely since χ^2 analyses have resulted in very low reduced χ^2 values for some of the models considered here, indicating that in this restricted parameter space the data sets are qualitatively consistent with each other given the error bars (Ganga et al. 1996; Lineweaver & Barbosa 1998; Tegmark 1998). Given that the field is still rapidly evolving, such differences are not unexpected.

Figure 6 shows the one-dimensional posterior distribution functions for $\Omega_B h^2$, derived by marginalizing the four-dimensional ones over the other three parameters. For both the flat- Λ and open models, and for all combined data sets considered, a low $\Omega_B h^2 \simeq 0.005$ is favored. While formal 2σ confidence upper limits exist (see Figure 6), the constraints derived from the gaussian posterior distribution ratio criterion discussed above are much weaker and do not rule out any value of $\Omega_B h^2$. Inclusion or exclusion of the SuZIE data do not significantly affect the deductions in this case.

While not very significant, it is gratifying that the CMB anisotropy data favor lower $\Omega_B h^2$, consistent with a number of recent estimates using different techniques, which disfavor $\Omega_B h^2$ larger than ~ 0.02 (e.g., Fukugita, Hogan, & Peebles 1998; Levshakov, Kegel, & Takahara 1998, but also see Burles & Tytler 1998). This low value for $\Omega_B h^2$ is also consistent with the indications from the Ganga et al. (1996) χ^2 analysis. However, it differs from the Lineweaver & Barbosa (1998) favored high value of $\Omega_B h^2 \simeq 0.026$.

Figure 7 shows the one-dimensional posterior distribution functions for t_0 , derived by marginalizing the four-dimensional ones over the other three parameters. For both the flat- Λ and open models, and for all combined data sets considered, a young universe, $t_0 \sim 10 - 12$ Gyr is favored. Again, while formal 2σ confidence upper limits exist (see Figure 7), constraints derived from the gaussian posterior distribution ratio criterion are much weaker, although they are stronger than for the case of $\Omega_B h^2$. These 1σ constraints are: for all the data and the open model, panel *b*), $t_0 \lesssim 16$ Gyr; for all the data excluding SuZIE and the open model, panel *d*), $t_0 \lesssim 19.5$ Gyr; and for the SP94Ka, MAX 4 ID, and MAX 5 HR combination, panels *e*) and *f*), $t_0 \lesssim 13.5$ Gyr ($t_0 \lesssim 15.5$ Gyr), for the flat- Λ (open) models. Inclusion or exclusion of the SuZIE data do not dramatically affect the deductions in this case.

Again, while not highly significant, it is gratifying that the CMB anisotropy data favor a young universe, consistent with other recent estimates (e.g., Feast & Catchpole 1997; Reid 1997; Gratton et al. 1997; Chaboyer et al. 1998). Lower t_0 corresponds to larger h . Hence these results would seem to be consistent with the indications for large h from the Ganga et al. (1996) χ^2 analysis. They also seem to be consistent with the open model values of $h \sim 0.6$ favored by Lineweaver & Barbosa (1998) and Baker et al. (1998). However, they would seem to be difficult to reconcile with the flat- Λ model value of $h \sim 0.35$ favored by Baker et al. (1998).

Figure 8 shows the one-dimensional posterior distribution functions for $Q_{\text{rms-PS}}$, derived by marginalizing the four-dimensional ones over the other three parameters. As discussed above, the three combined data sets result in fairly tight constraints on $Q_{\text{rms-PS}}$. At 2σ confidence they are consistent with the DMR results for both the open and flat- Λ models. However, at a lower level of confidence the DMR data favor a somewhat higher normalization for the flat- Λ model than do the small-scale data sets. This is consistent with indications from other data (e.g., Stompor et al. 1995; Liddle et al. 1996; Cole et al. 1997).

The peak values of the one-dimensional posterior distributions shown in Figures 5–8 are listed in the figure captions for the case when the four-dimensional posterior distributions are normalized such that $L(Q_{\text{rms-PS}} = 0 \mu\text{K}) = 1$. With this normalization, marginalizing over the remaining parameter the fully marginalized posterior distributions are, for the open (flat- Λ) models: $5 \times 10^{100}(9 \times 10^{100})$ for all the data; $4 \times 10^{100}(4 \times 10^{100})$ for all the data excluding SuZIE; and, $6 \times 10^{30}(6 \times 10^{30})$ for the SP94Ka, MAX 4 ID, and MAX 5 HR combination.

6. Conclusion

We have derived constraints on cosmological model parameters in the open and flat- Λ CDM models, from joint analyses of combinations of the SP94, ARGO, MAX 4+5, White Dish, and SuZIE CMB anisotropy data sets.

The favored value of Ω_0 in the open model depends sensitively on which combination of data is used. To determine if this is significant will require a models-based analysis of a larger number of data sets. Constraints on Ω_0 in the flat- Λ model, and constraints on $\Omega_B h^2$ and t_0 in both models, are only weakly dependent on the data set combination considered.

In the most conservative case, i.e., for the SP94Ka, MAX 4 ID, and MAX 5 HR data set combination, an open (flat- Λ) model with $\Omega_0 \simeq 0.1$ (1) is favored. We emphasize that, using the gaussian posterior ratio criterion, flat- Λ models with Ω_0 in the range from 0.1 to 1 cannot be ruled out at even 1σ confidence, although open models require $\Omega_0 \lesssim 0.3$ at 1σ confidence.

For both the open and flat- Λ models, and all data set combinations considered, low $\Omega_B h^2 \sim 0.005$, or young, $t_0 \sim 10$ Gyr, universes are weakly favored. This is in agreement with recent determinations based on other techniques.

It is gratifying that the small subset of current CMB anisotropy data considered in this paper can place some constraints on cosmological parameters. While these are mostly not very statistically significant, they are largely consistent with results determined using other, non-CMB anisotropy, measurements. To derive tighter and more robust constraints on cosmological parameters will require a models-based combined analysis of a much larger collection of CMB anisotropy data sets, including DMR.

We acknowledge useful discussions with C. Kochanek. We thank C. Lineweaver for a prompt, detailed and useful referee report, which helped improve the manuscript. This work was partially carried out at the Infrared Processing and Analysis Center and the Jet Propulsion Laboratory of the California Institute of Technology, under a contract with the National Aeronautics and Space Administration. KG also acknowledges support from NASA ADP grant NASA-1260. RS acknowledges support from a UK PPARC grant and from Polish Scientific Committee (KBN) grant 2P03D00813. BR and GR acknowledge support from NSF grant EPS-9550487 with matching support from the state of Kansas and from a K*STAR First award.

REFERENCES

- Anderson, G.W., & Carroll, S.M. 1998, in International Workshop on Particle Physics and the Early Universe, in press
- Bahcall, N.A., Fan, X., & Cen, R. 1997, *ApJ*, 485, L53
- Baker, J.C., et al. 1998, *MNRAS*, submitted
- Bartelmann, M., Huss, A., Colberg, J.M., Jenkins, A., & Pearce, F.R. 1998, *A&A*, 330, 1
- Bennett, C.L., et al. 1996, *ApJ*, 464, L1
- Bloomfield Torres, L.F., & Waga, I. 1996, *MNRAS*, 279, 712
- Bond, J.R., & Jaffe, A.H. 1997, in Microwave Background Anisotropies, ed. F. R. Bouchet, R. Gispert, B. Guiderdoni, & J. Tran Thanh Van (Gif-sur-Yvette: Editions Frontieres), 197
- Bond, J.R., Jaffe, A.H., & Knox, L. 1998, *Phys. Rev. D*, 57, 2117
- Borgani, S., et al. 1997, *ApJ*, 482, L121
- Bucher, M., Goldhaber, A.S., & Turok, N. 1995, *Phys. Rev. D*, 52, 3314
- Bunn, E.F., & Sugiyama, N. 1995, *ApJ*, 446, 49
- Burles, S., & Tytler, D. 1998, *ApJ*, 499, 699
- Caldwell, R.R., Dave, R., & Steinhardt, P.J. 1998, *Phys. Rev. Lett.*, 80, 1582
- Carlberg, R.G., Morris, S.L., Yee, H.K.C., & Ellingson, E. 1997b, *ApJ*, 479, L19
- Carlberg, R.G., et al. 1997a, *ApJ*, 476, L7
- Chaboyer, B., Demarque, P., Kernan, P.J., & Krauss, L.M. 1998, *ApJ*, 494, 96
- Cheng, E.S., et al. 1997, *ApJ*, 488, L59
- Cheng, Y.N., & Krauss, L.M. 1998, *MNRAS*, submitted
- Church, S.E., Ganga, K.M., Ade, P.A.R., Holzzapfel, W.L., Mauskopf, P.D., Wilbanks, T.M., & Lange, A.E. 1997, *ApJ*, 484, 523
- Coble, K., Dodelson, S., & Frieman, J.A. 1997, *Phys. Rev. D*, 55, 1851
- Cole, S., Weinberg, D.H., Frenk, C.S., & Ratra, B. 1997, *MNRAS*, 289, 37
- Colín, P., Klypin, A.A., Kravtsov, A.V., & Khokhlov, A.M. 1998, *ApJ*, submitted
- Croft, R.A.C., Weinberg, D.H., Pettini, M., Hernquist, L., & Katz, N. 1998, *ApJ*, submitted
- de Bernardis, P., et al. 1994, *ApJ*, 422, L33
- Della Valle, M., Kissler-Patig, M., Danziger, J., & Storm, J. 1998, *MNRAS*, 299, 267
- Deltorn, J.-M., Le Fèvre, O., Crampton, D., & Dickinson, M. 1997, *ApJ*, 483, L21
- de Oliveira-Costa, A., Devlin, M.J., Herbig, T., Miller, A.D., Netterfield, C.B., Page, L.A., & Tegmark, M. 1998, *ApJ*, 509, L77

- de Oliveira-Costa, A., Kogut, A., Devlin, M.J., Netterfield, C.B., Page, L.A., & Wollack, E.J. 1997, *ApJ*, 482, L17
- Donahue, M., Voit, G.M., Gioia, I., Luppino, G., Hughes, J.P., & Stocke, J.T. 1998, *ApJ*, 502, 550
- Ebeling, H., Edge, A.C., Fabian, A.C., Allen, S.W., Crawford, C.S., & Böhringer, H. 1997, *ApJ*, 479, L101
- Eke, V.R., Cole, S., Frenk, C.S., & Henry, J.P. 1998, *MNRAS*, 298, 1145
- Ettori, S., Fabian, A.C., & White, D.A. 1997, *MNRAS*, 289, 787
- Evrard, A.E. 1997, *MNRAS*, 292, 289
- Falco, E.E., Kochanek, C.S., & Muñoz, J.A. 1998, *ApJ*, 494, 47
- Falco, E.E., Shapiro, I.I., Moustakas, L.A., & Davis, M. 1997, *ApJ*, 484, 70
- Feast, M.W., & Catchpole, R.M. 1997, *MNRAS*, 286, L1
- Femenía, B., Rebolo, R., Gutiérrez, C.M., Limon, M., & Piccirillo, L. 1998, *ApJ*, 498, 117
- Ferreira, P.G., & Joyce, M. 1997, *Phys. Rev. Lett.*, 79, 4740
- Francis, P.J., Woodgate, B.E., & Danks, A.C. 1997, *ApJ*, 482, L25
- Frieman, J.A., & Waga, I. 1998, *Phys. Rev. D*, 57, 4642
- Fukugita, M., Hogan, C.J., & Peebles, P.J.E. 1998, *ApJ*, 503, 518
- Ganga, K., Page, L., Cheng, E., & Meyer, S. 1994, *ApJ*, 432, L15
- Ganga, K., Ratra, B., Church, S.E., Sugiyama, N., Ade, P.A.R., Holzappel, W.L., Mauskopf, P.D., & Lange, A.E. 1997b, *ApJ*, 484, 517
- Ganga, K., Ratra, B., Gundersen, J.O., & Sugiyama, N. 1997a, *ApJ*, 484, 7 (GRGS)
- Ganga, K., Ratra, B., Lim, M.A., Sugiyama, N., & Tanaka, S.T. 1998, *ApJS*, 114, 165
- Ganga, K., Ratra, B., & Sugiyama, N. 1996, *ApJ*, 461, L61
- Gardner, J.P., Sharples, R.M., Frenk, C.S., & Carrasco, B.E. 1997, *ApJ*, 480, L99
- Giovanelli, R., Haynes, M.P., da Costa, L.N., Freudling, W., Salzer, J.J., & Wegner, G. 1997, *ApJ*, 477, L1
- Górski, K.M., Banday A.J., Bennett, C.L., Hinshaw, G., Kogut, A., Smoot, G.F., & Wright, E.L. 1996, *ApJ*, 464, L11
- Górski, K.M., Ratra, B., Stompor, R., Sugiyama, N., & Banday, A.J. 1998, *ApJS*, 114, 1
- Górski, K.M., Ratra, B., Sugiyama, N., & Banday, A.J. 1995, *ApJ*, 444, L65
- Gott, J.R. 1982, *Nature*, 295, 304
- Governato, F., Babul, A., Quinn, T., Tozzi, P., Baugh, C.M., Katz, N., & Lake, G. 1998, *MNRAS*, submitted

- Gratton, R.G., Fusi Pecci, F., Carretta, E., Clementini, G., Corsi, C.E., & Lattanzi, M. 1997, *ApJ*, 491, 749
- Griffin, G.S., Nguyễn, H.T., Peterson, J.B., & Tucker, G.S. 1999, in preparation
- Gundersen, J.O., et al. 1995, *ApJ*, 443, L57
- Guth, A. 1981, *Phys. Rev. D*, 23, 347
- Guth, A.H., & Weinberg, E.J. 1983, *Nucl. Phys. B*, 212, 321
- Gutiérrez, C.M., et al. 1997, *ApJ*, 480, L83
- Hancock, S., Rocha, G., Lasenby, A.N., & Gutiérrez, C.M. 1998, *MNRAS*, 294, L1
- Harrison, E.R. 1970, *Phys. Rev. D*, 1, 2726
- Hjorth, J., & Tanvir, N.R. 1997, *ApJ*, 482, 68
- Huterer, D., & Turner, M.S. 1998, *Phys. Rev. Lett.*, submitted
- Jain, D., Panchapakesan, N., Mahajan, S., & Bhatia, V.B. 1998, *ApJ*, submitted
- Kazanas, D. 1980, *ApJ*, 241, L59
- Kochanek, C.S. 1996, *ApJ*, 466, 638
- Leitch, E.M., Readhead, A.C.S., Pearson, T.J., Myers, S.T., & Gulkis, S. 1998, *ApJ*, submitted
- Levshakov, S.A., Kegel, W.H., & Takahara, F. 1998, *ApJ*, 499, L1
- Liddle, A.R., Lyth, D.H., Viana, P.T.P., & White, M. 1996, *MNRAS*, 282, 281
- Lim, M.A., et al. 1996, *ApJ*, 469, L69
- Lineweaver, C.H., & Barbosa, D. 1998, *ApJ*, 496, 624
- Lineweaver, C.H., Barbosa, D., Blanchard, A., & Bartlett, J.G. 1997, *A&A*, 322, 365
- Maddox, S.J., Efstathiou, G., & Sutherland, W.J. 1996, *MNRAS*, 283, 1227
- Masi, S., de Bernardis, P., De Petris, M., Gervasi, M., Boscaleri, A., Aquilini, E., Martinis, L., & Scaramuzzi, F. 1996, *ApJ*, 463, L47
- Mushotzky, R.F., & Scharf, C.A. 1997, *ApJ*, 482, L13
- Netterfield, C.B., Devlin, M.J., Jarosik, N., Page, L., & Wollack, E.J. 1997, *ApJ*, 474, 47
- Özer, M., & Taha, M.O. 1998, *Mod. Phys. Lett. A*, 13, 571
- Park, C., Colley, W.N., Gott, J.R., Ratra, B., Spergel, D.N., & Sugiyama, N. 1998, *ApJ*, 506, 473
- Peebles, P.J.E. 1998, *Phil. Trans. R. Soc. Lond. A*, in press
- Peebles, P.J.E., & Ratra, B. 1988, *ApJ*, 325, L17
- Peebles, P.J.E., & Yu, J.T. 1970, *ApJ*, 162, 815
- Perlmutter, S., et al. 1999, *ApJ*, in press
- Platt, S.R., Kovac, J., Dragovan, M., Peterson, J.B., & Ruhl, J.E. 1997, *ApJ*, 475, L1

- Ratra, B., Ganga, K., Stompor, R., Sugiyama, N., de Bernardis, P., & Górski, K.M. 1999, ApJ, 510, in press (R99)
- Ratra, B., Ganga, K., Sugiyama, N., Tucker, G.S., Griffin, G.S., Nguyễn, H.T., & Peterson, J.B. 1998, ApJ, 505, 8
- Ratra, B., & Peebles, P.J.E. 1994, ApJ, 432, L5
- Ratra, B., & Peebles, P.J.E. 1995, Phys. Rev. D, 52, 1837
- Ratra, B., & Quillen, A. 1992, MNRAS, 259, 738
- Ratra, B., Sugiyama, N., Banday, A.J., & Górski, K.M. 1997, ApJ, 481, 22
- Reid, I.N. 1997, AJ, 114, 161
- Retzlaff, J., Borgani, S., Gottlöber, S., Klypin, A., & Müller, V. 1998, New Astron., 3, 631
- Riess, A.G., et al. 1998, AJ, 116, 1009
- Sato, K. 1981a, Phys. Lett. B, 99, 66
- Sato, K. 1981b, MNRAS, 195, 467
- Small, T.A., Ma, C.-P., Sargent, W.L.W., & Hamilton, D. 1998, ApJ, 492, 45
- Small, T.A., Sargent, W.L.W., & Hamilton, D. 1997, ApJ, 487, 512
- Smoot, G.F., et al. 1992, ApJ, 396, L1
- Starobinsky, A.A. 1998, JETP Lett., 68, 757
- Stompor, R. 1994, A&A, 287, 693
- Stompor, R. 1997, in Microwave Background Anisotropies, ed. F.R. Bouchet, R. Gispert, B. Guiderdoni, & J. Tran Thanh Van (Gif-sur-Yvette: Editions Frontieres), 91
- Stompor, R., Górski, K.M., & Banday, A.J. 1995, MNRAS, 277, 1225
- Subrahmanyam, R., Kesteven, M.J., Ekers, R.D., Sinclair, M., & Silk, J. 1998, MNRAS, 298, 1189
- Sugiyama, N. 1995, ApJS, 100, 281
- Sugiyama, N., & Sato, K. 1992, ApJ, 387, 439
- Tegmark, M. 1998, ApJ, submitted
- Tanaka, S.T., et al. 1996, ApJ, 468, L81
- Tucker, G.S., Griffin, G.S., Nguyễn, H.T., & Peterson, J.B. 1993, ApJ, 419, L45
- Tucker, G.S., Gush, H.P., Halpern, M., Shinkoda, I., & Towlson, W. 1997, ApJ, 475, L73
- van Dokkum, P.G., Franx, M., Kelson, D.D., & Illingworth, G.D. 1998, ApJ, 504, L17
- Viana, P.T.P., & Liddle, A.R. 1998, Phys. Rev. D, 57, 674
- Vogt, N.P., Forbes, D.A., Phillips, A.C., Gronwall, C., Faber, S.M., Illingworth, G.D., & Koo, D.C. 1996, ApJ, 465, L15

- Voit, G.M., & Donahue, M. 1998, ApJ, 500, L111
Willick, J.A., Strauss, M.A., Dekel, A., & Kolatt, T. 1997, ApJ, 486, 629
Wright, E.L., et al. 1992, ApJ, 396, L13
Yamamoto, K., & Bunn, E.F. 1996, ApJ, 464, 8
Yamamoto, K., Sasaki, M., & Tanaka, T. 1995, ApJ, 455, 412
Zel'dovich, Ya. B. 1972, MNRAS, 160, 1P

Figure Captions

Fig. 1.– CMB anisotropy multipole moments $l(l+1)C_l/(2\pi) \times 10^{10}$ as a function of multipole l , for selected models normalized to the DMR data (Górski et al. 1998; Stompor 1997). Panels *a) – c)* show selected flat- Λ models. The heavy lines are the $\Omega_0 = 1$, $\Omega_B h^2 = 0.005$, and $t_0 = 10$ Gyr case, which is close to where the SP94Ka, MAX 4 ID, and MAX 5 HR data set combination posterior density distributions (marginalized over all but one parameter at a time) are at a maximum. Panel *a)* shows five $\Omega_B h^2 = 0.005$, $t_0 = 10$ Gyr models with $\Omega_0 = 0.2, 0.4, 0.6, 0.8$, and 1 in descending order at the $l \sim 200$ peaks. Panel *b)* shows seven $\Omega_0 = 1$, $t_0 = 10$ Gyr models with $\Omega_B h^2 = 0.029, 0.025, 0.021, 0.017, 0.013, 0.009$, and 0.005 in descending order at the $l \sim 200$ peaks. Panel *c)* shows six $\Omega_0 = 1$, $\Omega_B h^2 = 0.005$ models with $t_0 = 20, 18, 16, 14, 12$, and 10 Gyr in descending order at the $l \sim 200$ peaks. Panels *d) – f)* show selected open models. The heavy lines are the $\Omega_0 = 0.1$, $\Omega_B h^2 = 0.005$, and $t_0 = 10$ Gyr case, which is close to where the SP94Ka, MAX 4 ID, and MAX 5 HR data set combination posterior density distributions (marginalized over all but one parameter at a time) are at a maximum. Panel *d)* shows five $\Omega_B h^2 = 0.005$, $t_0 = 10$ Gyr models with $\Omega_0 = 0.9, 0.7, 0.5, 0.3$, and 0.1 from left to right at the peaks. Panel *e)* shows seven $\Omega_0 = 0.1$, $t_0 = 10$ Gyr models with $\Omega_B h^2 = 0.029, 0.025, 0.021, 0.017, 0.013, 0.009$, and 0.005 in descending order at $l \sim 600$. Panel *f)* shows six $\Omega_0 = 0.1$, $\Omega_B h^2 = 0.005$ models with $t_0 = 20, 18, 16, 14, 12$, and 10 Gyr in descending order at $l \sim 600$.

Fig. 2.– Confidence contours and maxima of the two-dimensional posterior probability density distribution functions, as a function of the two parameters on the axes of each panel (derived by marginalizing the four-dimensional posterior distributions over the other two parameters). Dashed lines (crosses) show the contours (maxima) of the open case and solid lines (solid circles) show those of the flat- Λ model. Contours of $0.25, 0.5, 1, 2$, and 3σ confidence are shown (some contours are not labelled). Panels *a) – c)* in the left column show the $(\Omega_B h^2, \Omega_0)$ plane, while panels *d) – f)* in the right column show the (t_0, Ω_0) plane. Panels *a)* & *d)* in the top row are from an analysis of all the small scale data. Panels *b)* & *e)* in the middle row are from an analysis of all but the SuZIE small scale data. Panels *c)* & *f)* in the bottom row are from an analysis of the SP94Ka, MAX 4 ID, and MAX 5 HR data sets.

Fig. 3.– Confidence contours and maxima of the two-dimensional $(Q_{\text{rms-PS}}, \Omega_0)$ posterior probability density distribution functions. Panels *a), c), & e)* in the left column show the flat- Λ model and panels *b), d), & f)* in the right column show the open model. Note the different scale on the vertical ($Q_{\text{rms-PS}}$) axes of pairs of panels in each row. Shaded regions and those enclosed by thin solid lines show the results derived from the various combination data sets considered. Densest shading shows the 1σ confidence region, less-dense shading shows the 2σ region, and thin solid lines enclose the 3σ region. Solid circles show the maxima of the two-dimensional posterior distributions. Heavy lines show the two-dimensional posterior probability density distribution function 1 and 2σ confidence limits for the DMR data (Górski et al. 1998; Stompor 1997). The DMR results are a composite of those from analyses of the two extreme data sets: i) galactic frame

with quadrupole included and correcting for faint high-latitude galactic emission; and ii) ecliptic frame with quadrupole excluded and no other galactic emission correction (Górski et al. 1998). Panels *a*) & *b*) in the top row are from an analysis of all the small scale data. Panels *c*) & *d*) in the middle row are from an analysis of all but the SuZIE small scale data. Panels *e*) & *f*) in the bottom row are from an analysis of the SP94Ka, MAX 4 ID, and MAX 5 HR data sets.

Fig. 4.– Confidence contours and maxima of the two-dimensional $(Q_{\text{rms-PS}}, \Omega_0)$ posterior probability density distribution functions for the open model. Conventions are as described in the caption of Figure 3. Panel *a*) is from an analysis of the MAX 4 ID data, panel *b*) from the MAX 5 HR data, and panel *c*) from the SP94Ka data. Panel *d*) is from a combined analysis of the SP94Ka, MAX 4 ID, and MAX 5 HR data sets. Note the different scale on the vertical ($Q_{\text{rms-PS}}$) axis in panel *a*).

Fig. 5.– One-dimensional posterior probability density distribution functions for Ω_0 , derived by marginalizing the four-dimensional ones over the other three parameters, in the open and flat- Λ models. These have been renormalized to unity at the peaks. Dotted lines show the formal 1 and 2 σ confidence limits derived from these one-dimensional posterior distributions. Panels *a*), *c*), & *e*) in the left column show the flat- Λ model and panels *b*), *d*), & *f*) in the right column show the open model. Panels *a*) & *b*) in the top row are from an analysis of all the small scale data. Panels *c*) & *d*) in the middle row are from an analysis of all but the SuZIE small scale data. Panels *e*) & *f*) in the bottom row are from an analysis of the SP94Ka, MAX 4 ID, and MAX 5 HR data sets. When the four-dimensional posterior distributions are normalized such that $L(Q_{\text{rms-PS}} = 0 \mu\text{K}) = 1$, the peak values of the one-dimensional distributions shown in panels *a*) – *f*) are 1×10^{101} , 1×10^{101} , 4×10^{100} , 6×10^{100} , 6×10^{30} , and 1×10^{31} , respectively.

Fig. 6.– One-dimensional posterior probability density distribution functions for $\Omega_B h^2$, derived by marginalizing the four-dimensional ones over the other three parameters, in the open and flat- Λ models. Conventions are as described in the caption of Figure 5. When the four-dimensional posterior distributions are normalized such that $L(Q_{\text{rms-PS}} = 0 \mu\text{K}) = 1$, the peak values of the one-dimensional distributions shown in panels *a*) – *f*) are 4×10^{102} , 3×10^{102} , 2×10^{102} , 2×10^{102} , 3×10^{32} , and 3×10^{32} , respectively.

Fig. 7.– One-dimensional posterior probability density distribution functions for t_0 , derived by marginalizing the four-dimensional ones over the other three parameters, in the open and flat- Λ models. Conventions are as described in the caption of Figure 5. When the four-dimensional posterior distributions are normalized such that $L(Q_{\text{rms-PS}} = 0 \mu\text{K}) = 1$, the peak values of the one-dimensional distributions shown in panels *a*) – *f*) are 1×10^{100} , 8×10^{99} , 4×10^{99} , 5×10^{99} , 1×10^{30} , and 8×10^{29} , respectively.

Fig. 8.– One-dimensional posterior probability density distribution functions for $Q_{\text{rms-PS}}$, derived by marginalizing the four-dimensional ones over the other three parameters, in the open and

flat- Λ models. Conventions are as described in the caption of Figure 5. Also shown here, as dotted lines, are the formal 3σ confidence limits derived from these one-dimensional posterior distributions. Solid vertical lines show the ± 1 and $\pm 2\sigma$ confidence limits derived by projecting the corresponding small-scale data four-dimensional posterior distributions. Also shown are the 2σ DMR (marginalized and projected) confidence limits; these are a composite of those from the two extreme DMR data sets (see caption of Figure 3). When the four-dimensional posterior distributions are normalized such that $L(Q_{\text{rms-PS}} = 0 \mu\text{K}) = 1$, the peak values of the one-dimensional distributions shown in panels *a) – f)* are 2×10^{100} , 9×10^{99} , 8×10^{99} , 4×10^{99} , 8×10^{29} , and 4×10^{29} , respectively.

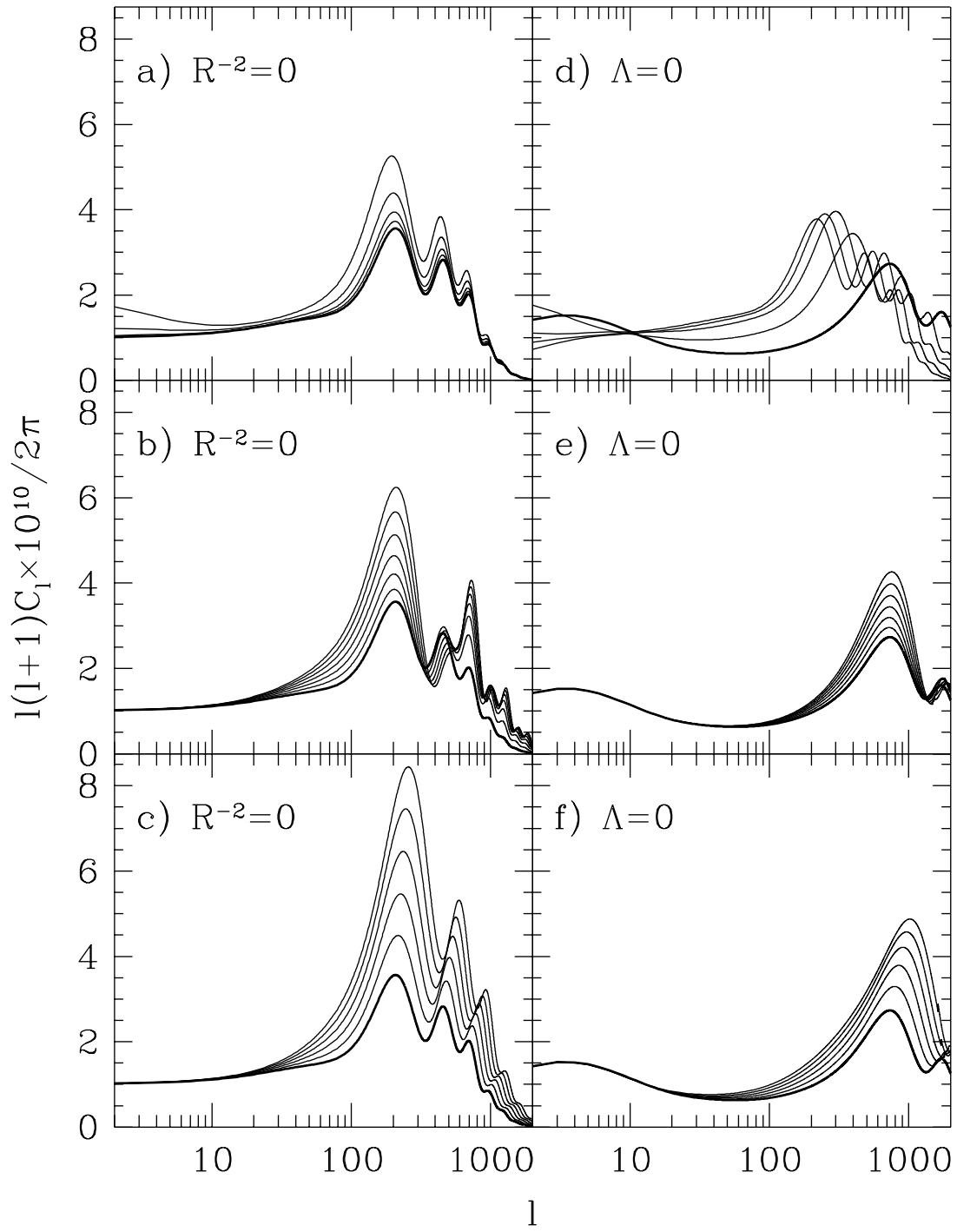


Figure 1

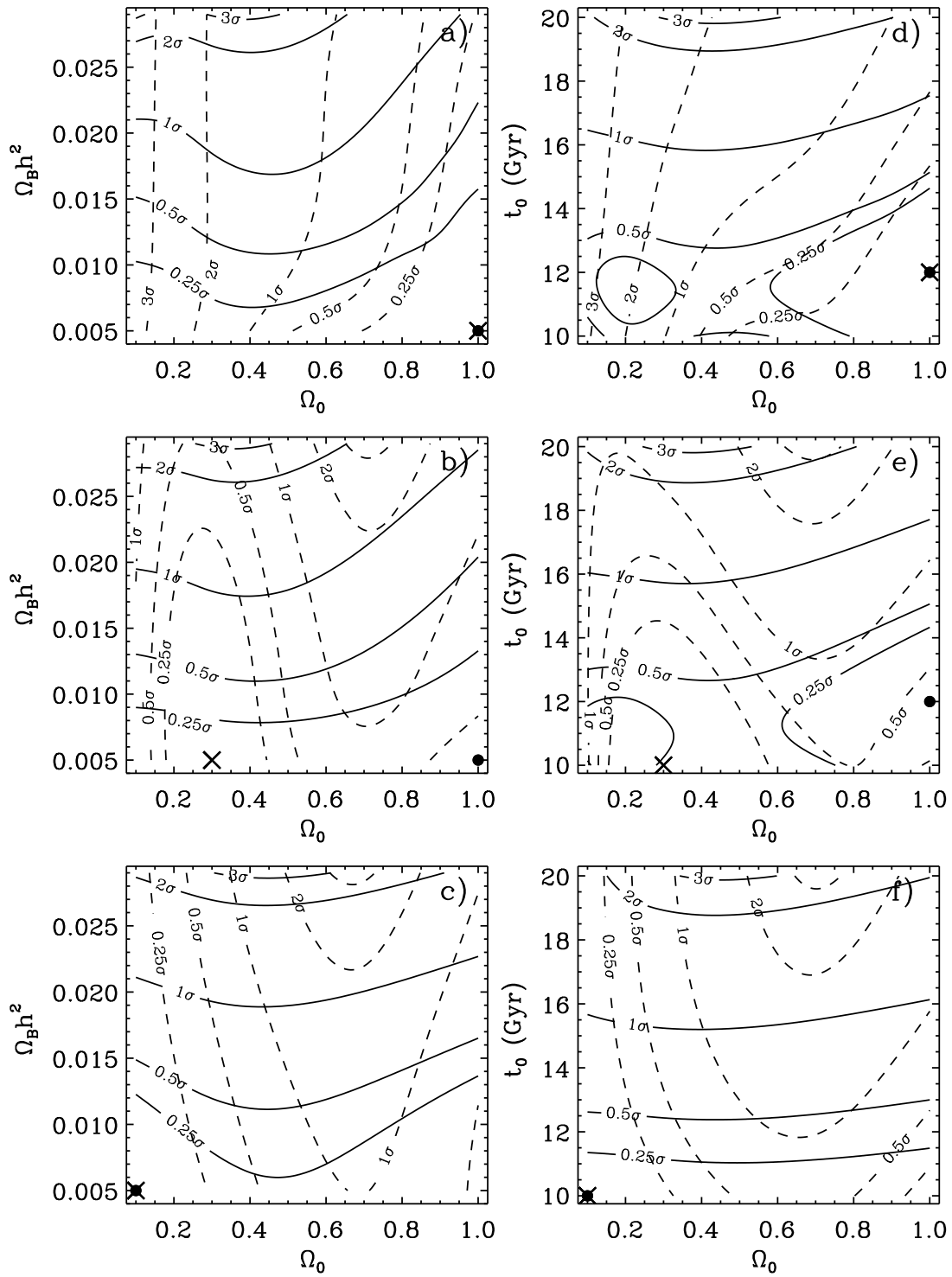


Figure 2

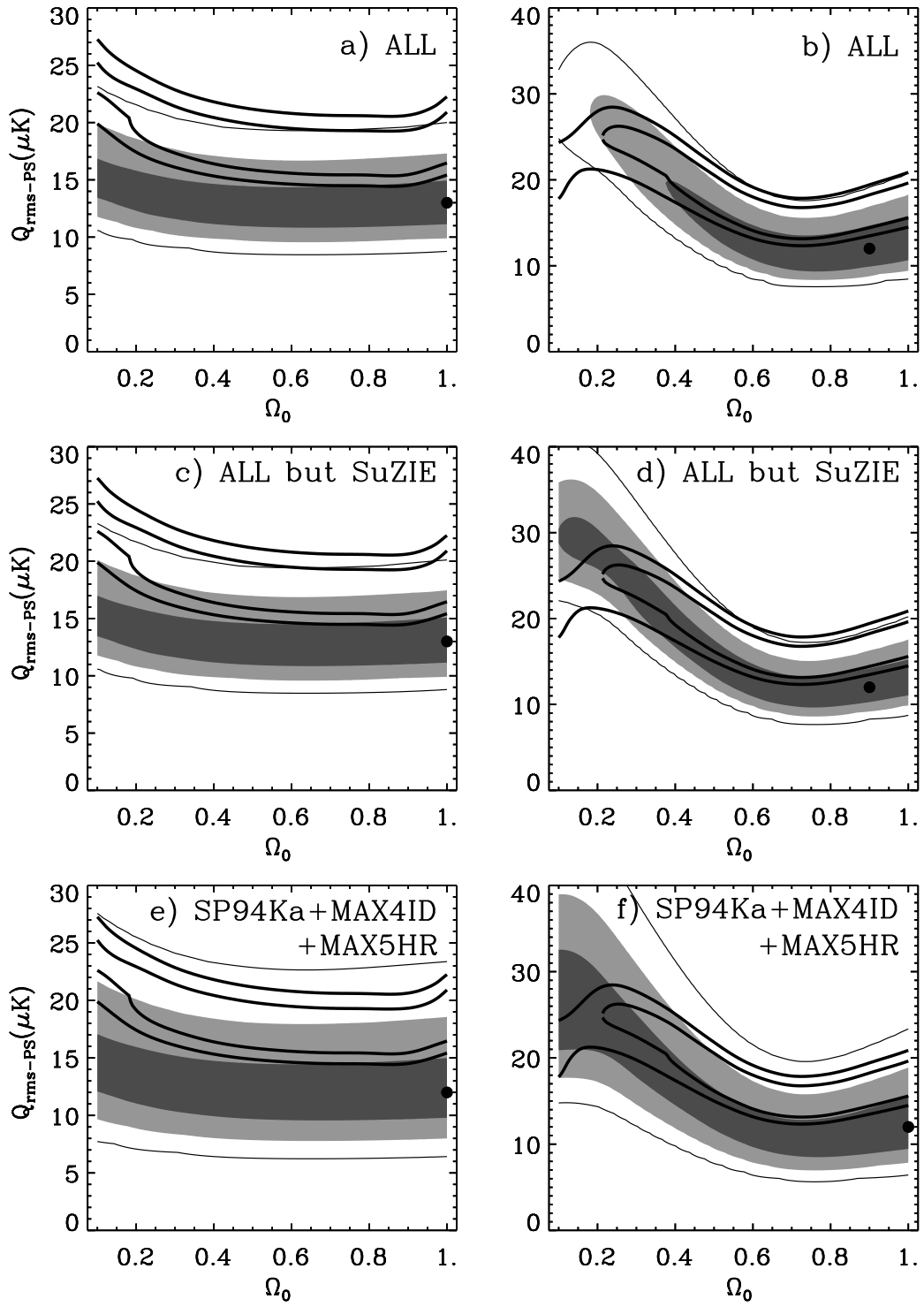


Figure 3

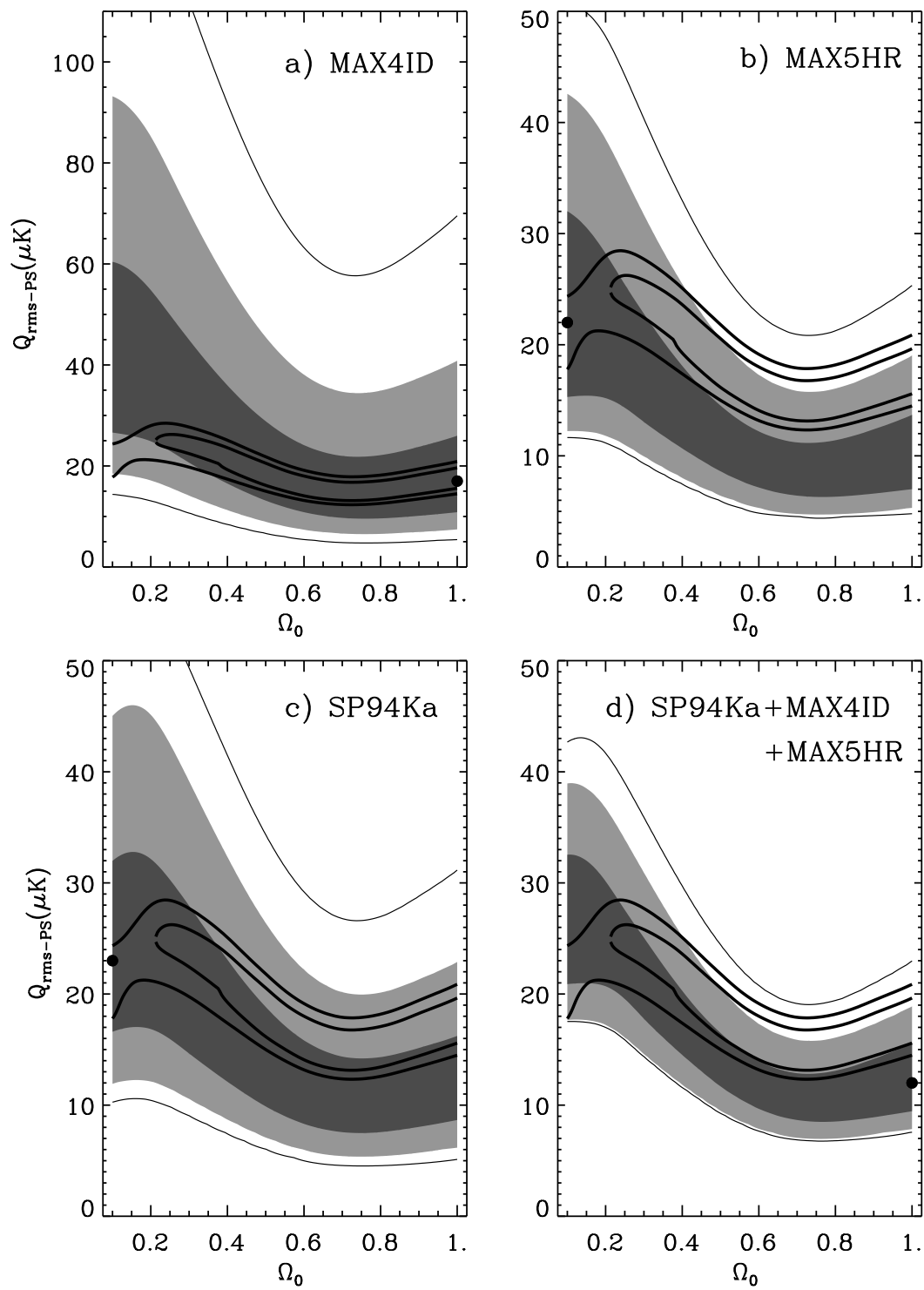


Figure 4

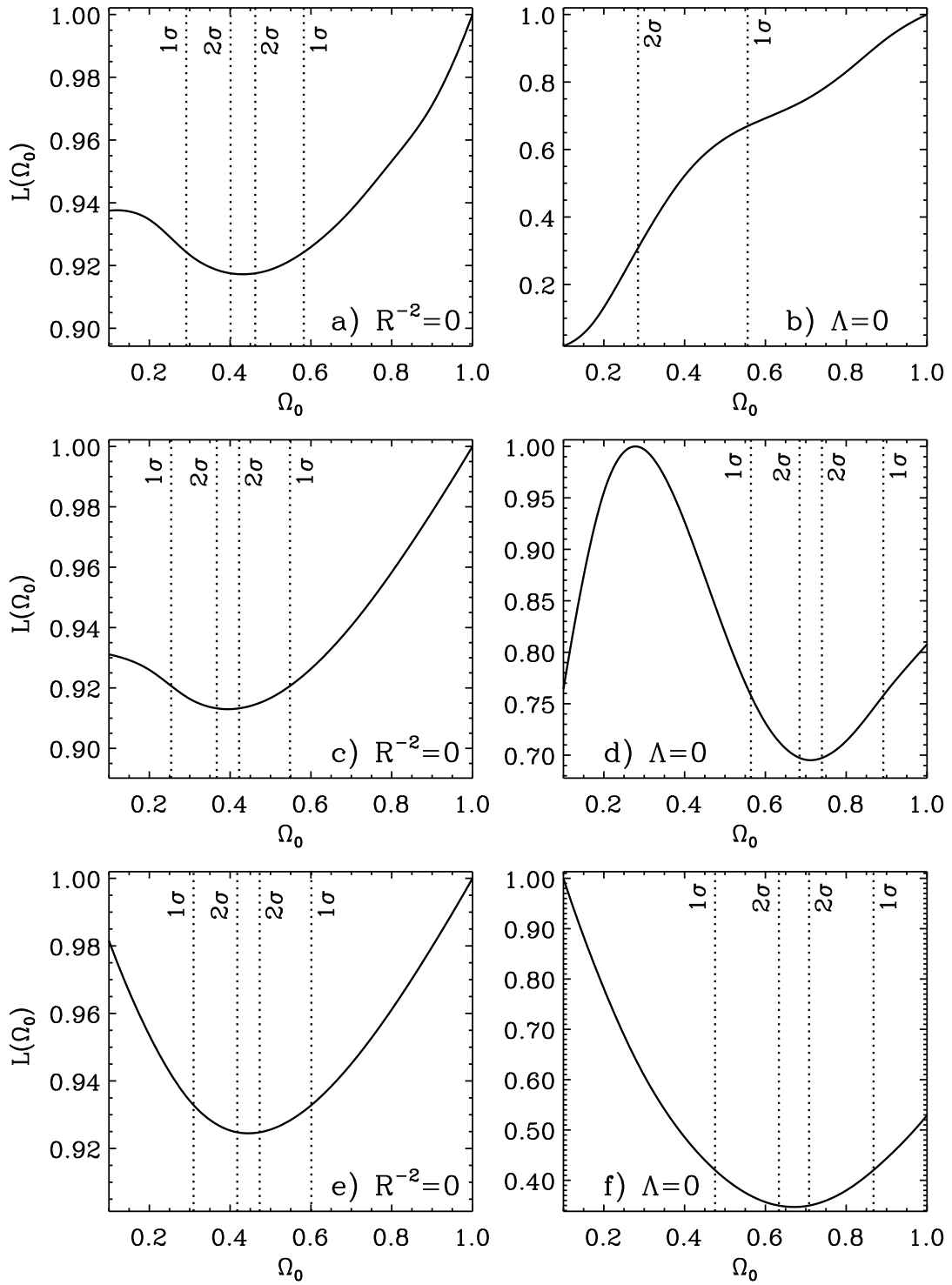


Figure 5

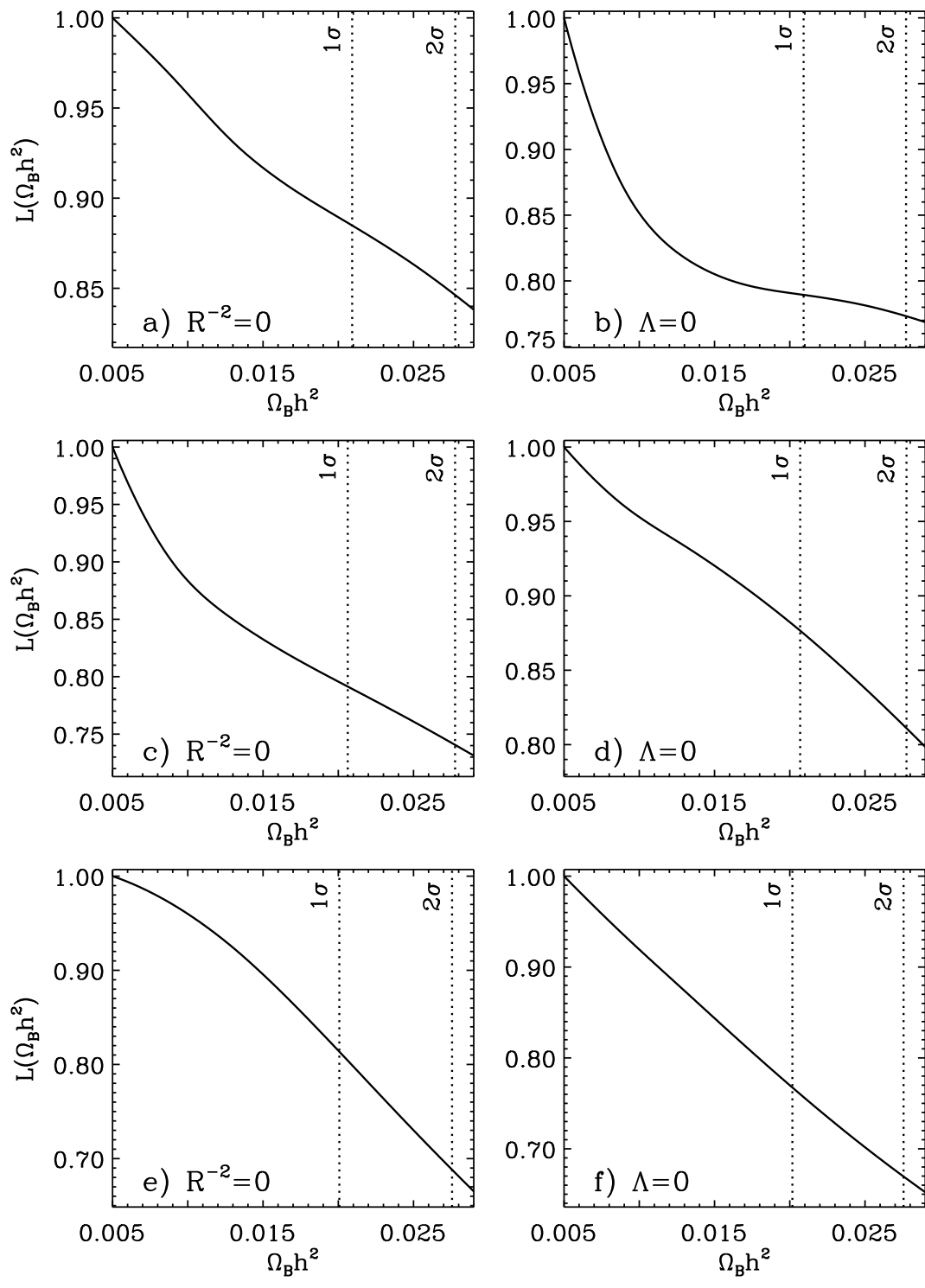


Figure 6

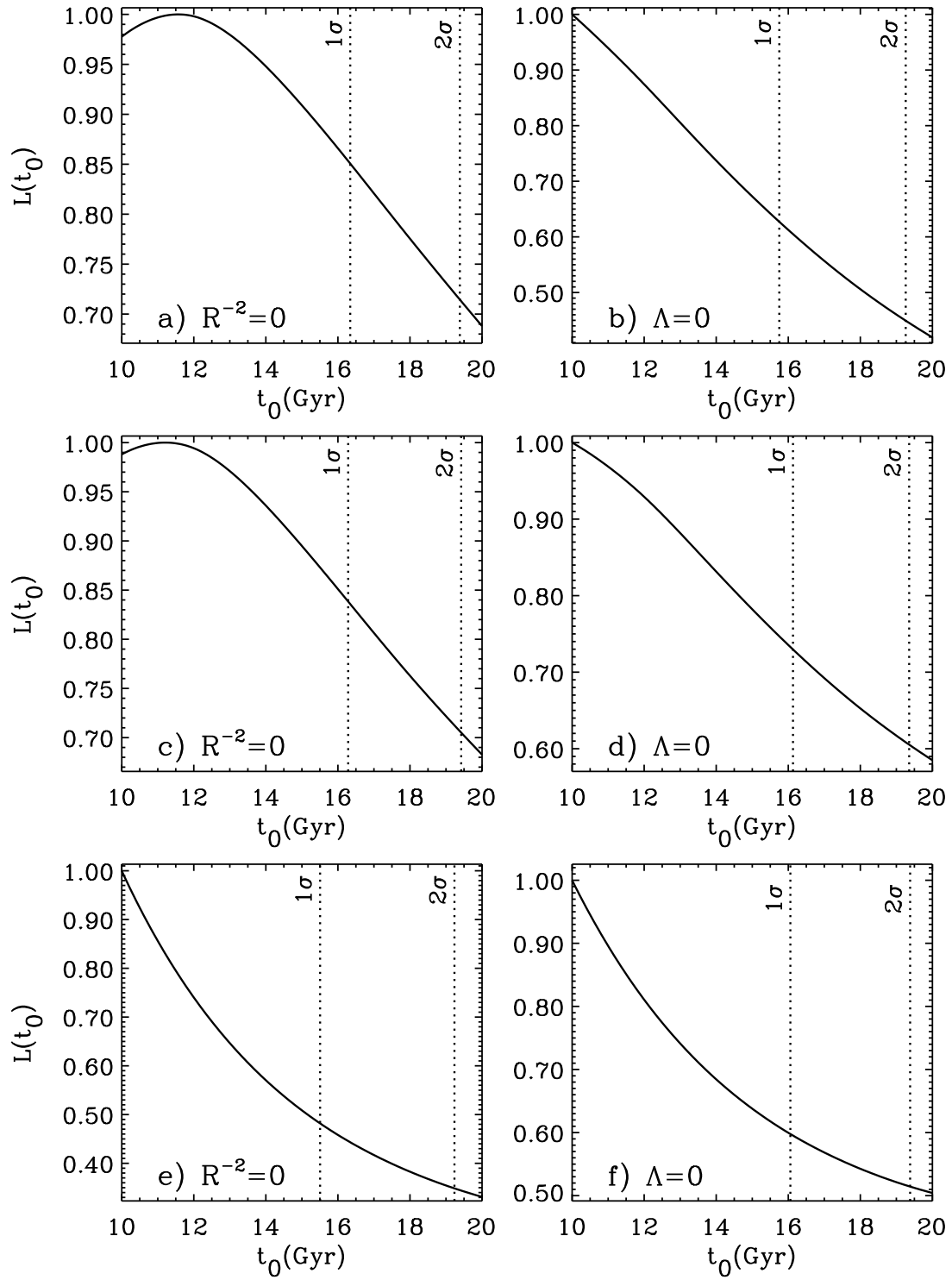


Figure 7

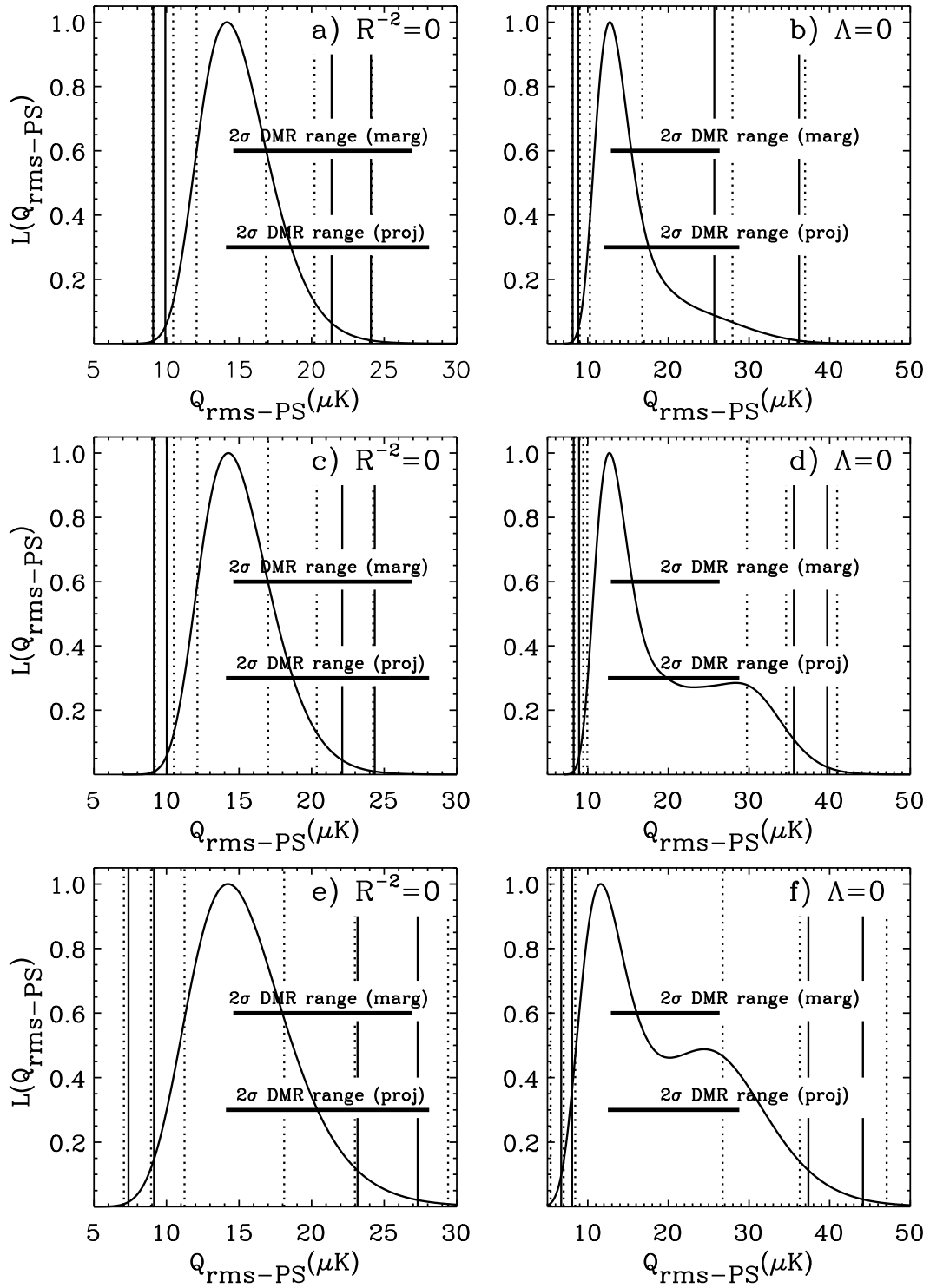


Figure 8